Hyperfine Interact (2015) 230:195–203
DOI 10.1007/s10751-014-1092-x

A Mössbauer investigation of orthorhombic phase YbMnO3

G. A. Stewart · H. A. Salama · C. J. Voyer · D. H. Ryan · D. Scott · H. StC. O'Neill

Published online: 18 November 2014

Abstract ^{170}Yb- and ^{57}Fe-Mössbauer spectra are reported for orthorhombic phase manganites $YbMnO_3$ and Yb($^{57}Fe_{0.005}Mn_{0.995}$)$O_3$, respectively. Point charge model estimates of the electric field gradient agree well with experimental ^{57}Fe-Mössbauer results in terms of both sign and magnitude of the electric quadrupole interaction strength, and the orientation of the magnetic hyperfine field is consistent with an E-type antiferromagnetic order where Mn moments are aligned along the *a*-axis (Pnma notation). The ^{170}Yb-Mössbauer spectra exhibit pure quadrupole splitting down to 1.8 K, contradicting an earlier report that the Yb sub-lattice orders in it own right at $T_{Yb} \approx 4$ K. Nevertheless, there is a slight increase in line broadening with decreasing temperature, probably due to the weak magnetic exchange field arising out of the ordered Mn sub-lattice. The small variation with temperature of the quadrupole interaction strength suggests that the Yb^{3+} electronic ground state is a well-isolated Kramers doublet.

Keywords Orthorhombic $YbMnO_3$ · Magnetisation · ^{57}*Fe*- and ^{170}*Yb*-Mössbauer · Spectroscopy

Proceedings of the 5th Joint International Conference on Hyperfine Interactions and International Symposium on Nuclear Quadrupole Interactions (HFI/NQI 2014) Canberra, Australia, 21–26 September 2014

G. A. Stewart · H. A. Salama
School of Physical, Environmental and Mathematical Sciences, UNSW Canberra at the Australian Defence Force Academy, Canberra BC, ACT 2610, Australia
e-mail: G.Stewart@adfa.edu.au

C. J. Voyer · D. H. Ryan
Centre for Physics of Materials and Department of Physics, McGill University, Montreal, Quebec, H3A 2T8, Canada

D. Scott · H. StC. O'Neill
Research School of Earth Sciences, The Australian National University, Canberra, ACT 0200, Australia

1 Introduction

The $RMnO_3$ (R = rare earth) family has the orthorhombic, perovskite-related, $GdFeO_3$-type structure for the larger rare-earth atoms La - Dy and a hexagonal structure for the smaller rare earths Ho - Lu. However, the hexagonal compounds can be converted to their orthorhombic polymorphs via quenching from a high pressure anneal. According to the extended magnetic phase diagram published by Tachibana et al.[1], the Mn sub-lattice of orthorhombic o-$YbMnO_3$ is expected to order with an incommensurate sinusoidal structure at $T_N \approx 43$ K and then lock in to a commensurate E-type antiferromagnetic arrangement below $T_{N'} \approx 36$ K. This E-type order has been confirmed by the low temperature neutron diffraction data of Huang et al. [2]. Using the Pnma setting, it equates to Mn moments aligned with the *a*-axis. On the basis of magnetic susceptibility data, the same authors proposed that the Yb sub-lattice orders in its own right below $T_{Yb} \approx 4$ K.

Here we probe the local magnetisation of the Mn and Yb sub-lattices of o-$YbMnO_3$ using ^{57}Fe- and ^{170}Yb-Mössbauer spectroscopy. To facilitate the ^{57}Fe measurements a dilute concentration of enriched ^{57}Fe is substituted into the Mn sub-lattice.

2 Experimental details

Hexagonal phase compounds $YbFe_xMn_{1-x}O_3$ (x = 0, 0.05) were prepared by conventional solid state reaction of stoichiometric amounts of Yb_2O_3 (99.9 %), Fe_2O_3 (99+ %) and $MnCO_3$ (99.9 %) as described previously [3]. The Fe_2O_3 employed was enriched to 96 at. % ^{57}Fe (compared with the natural isotopic abundance of just 2.2 at. %). These were then used as the starting material for synthesis of the orthorhombic phases using a high-pressure, piston cylinder apparatus. Lots of 100 – 250 mg of powdered material were sealed (by welding) in a platinum capsule and assembled into a hydraulic press. They were then annealed at 1000 °C and 3.5 GPa (35 kbar) for 10 h prior to quenching to room temperature.

X-ray powder diffraction patterns recorded using CuK_α radiation were consistent with a single orthorhombic phase for both specimens. Using the atomic position parameters from the room temperature neutron diffraction data of Huang et al. [2], the refined lattice parameters *a*, *b*, and *c* were respectively 0.57923, 0.73032 and 0.52155 nm for pure o-$YbMnO_3$ and 0.57991, 0.73032 and 0.52182 nm for the specimen doped with ^{57}Fe. The change brought about by the ^{57}Fe substitution is minor with cell constants and volume increased by less than 0.2 %.

The ^{57}Fe-Mössbauer spectra were recorded using a commercial ^{57}Co:Rh source mounted outside the cryostat at room temperature. The absorbers were comprised of $\approx$ 40 mg cm^{-2} of specimen material diluted with CB_4 and the drive velocity was calibrated against the room temperature α-Fe spectrum. For the acquisition of ^{170}Yb-Mössbauer spectra, both the source and absorber ($\approx$600 mg cm^{-2}) were mounted vertically inside a helium-flow cryostat. The 20 mCi ^{170}Tm source was prepared by neutron activation of $\approx$25 mg of Tm(10 wt. %)Al alloy and the drive velocity calibrated using a laser interferometer mounted on the back of the drive.

3 Point charge calculations

Simple point charge model (PCM) calculations were performed in order to assist with the analysis and interpretation of the experimental ^{57}Fe- and ^{170}Yb-Mössbauer spectra. For this

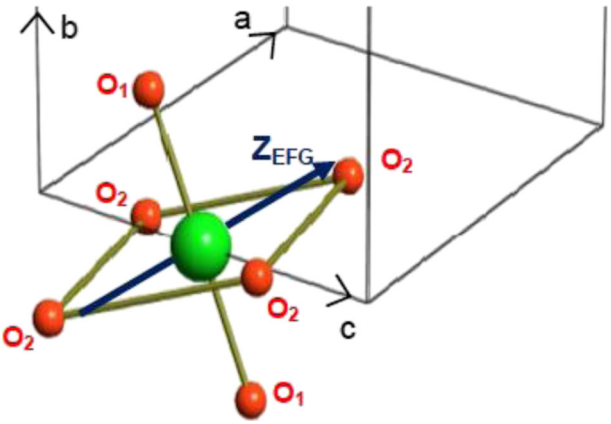

Fig. 1 Local octahedral environment for the Mn^{3+} (4b) site in o-$YbMnO^3$

purpose, the o-$YbMnO_3$ atomic position parameters were taken from the 9 K and 298 K neutron diffraction pattern refinements of Huang et al. [2].

The single Mn 4b-site has triclinic $\bar{1}$ (C_i) point symmetry and is located at the centre of a tilted, octahedral arrangement of oxygen ions (Fig. 1). Given that the substituted Fe^{3+} ions and the host Mn^{3+} ions are of comparable radius for six-fold oxygen co-ordination ($r_{Fe^{3+}} \approx r_{Mn^{3+}} \approx 0.0645$ nm [4]), it is reasonable to assume that the host Mn site is not distorted by Fe^{3+} substitution. Furthermore, $Fe^{3+}$is an S state ion with a negligible 3d shell contribution to the electric field gradient (EFG) at the ^{57}Fe nucleus. The lattice contribution to the EFG was estimated using a PCM summation over the six nearest O^{2-}neighbours, enhanced by a shielding factor of 1 - $\gamma\infty \approx 10$ [5, 6]). Because of the site's low symmetry, the principal EFG axes, $(x, y, z)_{EFG}$, are related to the crystal axes a, b, c via a coordinate frame rotation. The estimated Euler angles indicate that the Z_{EFG} axis is directed close to the direction of the longer Mn-O2 bond. However, in the context of the E-type magnetic structure, it is the orientation of the crystal a-axis (the Mn moment axis) that is important. Based on the Euler angles, it was deduced to have polar coordinates of $\theta \approx 37.8$ ° and $\phi \approx 250°$ expressed with respect to the principal EFG axes frame. Finally, using $E\gamma$ =14.412 keV and the recommended quadrupole moment of $Q(^{57}Fe, I = 3/2) = +0.21(1)$ b [7, 8], the low temperature quadrupole interaction strength at the ^{57}Fe probe nuclei is estimated to be $eQV_{zz} = +2.66(13)$ mm s^{-1}. The PCM values of V_{ZZ}, eQV_{zz} the asymmetry parameter η, and the a-axis polar angles, θ and ϕ are presented in Table 1 for 9 and 298 K. As a cautionary observation, more recently reported values of $Q \approx 0.14 - 0.16$ b [e.g. 9, 10] would lead to smaller estimates of eQV_{zz}.

The single Yb 4c-site has monoclinic m(C_s) point symmetry which requires a crystal field (CF) Hamiltonian with 15 CF parameters to describe its interaction with the $^4F_{7/2}$ ground term of the Yb^{3+} 4f shell. The only experimentally determined CF parameters available for $YbMnO_3$ are those reported by Divis et al. [11] for the hexagonal phase. However, in that case, comparison with appropriately rotated PCM-estimates of the CF parameters revealed an approximately consistent scaling within each rank. The single rank 2 CF parameter, (Stevens notation), was about 2/3 of its PCM estimate. The rank 4 and rank 6 parameters were overall about 1–2 and 3–5 times larger, respectively. This suggested an approach for arriving at a tentative set of CF parameters for the Yb-site in o-$YbMnO_3$. The CF parameters were estimated using a PCM summation over a sphere of radius r >

Table 1 ^{57}Fe-Mössbauer spectroscopy results for orthorhombic Yb($^{57}Fe_{0.005}Mn_{0.995}$)$O_3$. They include the isomer shift, δ (expressed relative to α-Fe at room temperature), FWHM line width, Γ, quadrupole interaction strength, eQV_{zz}, asymmetry parameter, η, paramagnetic doublet splitting, ΔE_Q, magnetic hyperfine field, B_{hf}, and polar coordinates, θ and ϕ, defining orientation with respect to the EFG tensor's principal axes. Point charge model (PCM) estimates are included for ease of comparison

T (K)	δ (mm s^{-1})	Γ (mm s^{-1})	eQV_{zz} (mm s^{-1})	η	ΔE_Q (mm s^{-1})	B_{hf} (T)	θ (°)	ϕ (°)
PCM theory								
298			+2.68	0.25	1.35[a]			
9			+2.66	0.175			37.8[b]	≈ 250[b]
^{57}Fe-Mössbauer spectroscopy								
300	0.357(3)	0.35(2)			1.54(2)			
4.2	0.47(1)	0.37(3)	+3.40(2)	0.175[d]		44.7(4)	37.8[c,d]	270(10)[c]

[a] $\Delta E_Q = 1/2eQV_{zz}(1 + 1/3\eta^2)^{1/2}$

[b] Orientation of crystal *a*-axis

[c] Orientation of B_{hf}

[d] Fixed parameters, based on agreement with PCM orientation of crystal *a*-axis

50 a, (a is the lattice parameter). Then they were scaled using the above factors derived for h–$YbMnO_3$ to give $\boldsymbol{B_n^m} \approx -3.15$ K (n = 2, m = 0), −3.83 K (2,2), +5.50 K (2,−2), −4.02 mK (4,0), +99.0 mK (4,2), −0.632 K (4,−2), +0.530 K (4,4), +1.62 K (4,−4), −2.62 mK (6,0), +19.8 mK (6,2), +8.91 mK (6,−2), −62.4 mK (6,4), +6.21 mK (6,−4), +3.81 mK (6,6) and +2.66 mK (6,−6).

4 Results and discussion

The ^{57}Fe-Mössbauer spectra recorded for the ^{57}Fe-doped o-$YbMnO_3$ specimen are shown in Fig. 2 as a function of temperature (4.2 – 300 K). At the extremes of the temperature range, the spectra are relatively straightforward. The room temperature spectrum is a single paramagnetic doublet and the 4.2 K spectrum is a single magnetic sextet. However, in order to achieve an acceptable fit with a similar quadrupole interaction strength, eQV_{zz}, at the two temperatures, it was necessary to direct the magnetic hyperfine field, B_{hf}, at a polar angle of θ = 35 – 40° away from z_{EFG}. This θ range is centred on the theoretical PCM value of θ ≈ 37.8° that was determined in Section 3 for the alignment of the *a*-axis with respect to z_{EFG}. Thus the alignment of the E-type Mn magnetic moments (and the ^{57}Fe hyperfine field B_{hf}) with the crystal *a*-axis is supported by the ^{57}Fe-Mössbauer measurements. The fit of the 4.2 K spectrum was then refined using the fixed PCM values of η = 0.175 and θ ≈ 37.8°. The final sets of parameters fitted to the room temperature and 4.2 K spectra using this approach are given in the lower half of Table 1. The 4.2 K value of B_{hf} = 44.7 T is typical for the high spin S = 5/2 state of Fe^{3+}.

For intermediate temperatures, the ^{57}Fe-Mössbauer spectra are evidently more complicated. The paramagnetic doublets (solid green theory curves in Fig. 2) persist in isolation from room temperature down to the onset of the incommensurate sinusoidal magnetic order at $T_N \approx 43$ K. Similarly the magnetic sextets (red theory curves in Fig. 2) persist, with reducing magnetic splitting, as the temperature increases from 4.2 K up to the lock in

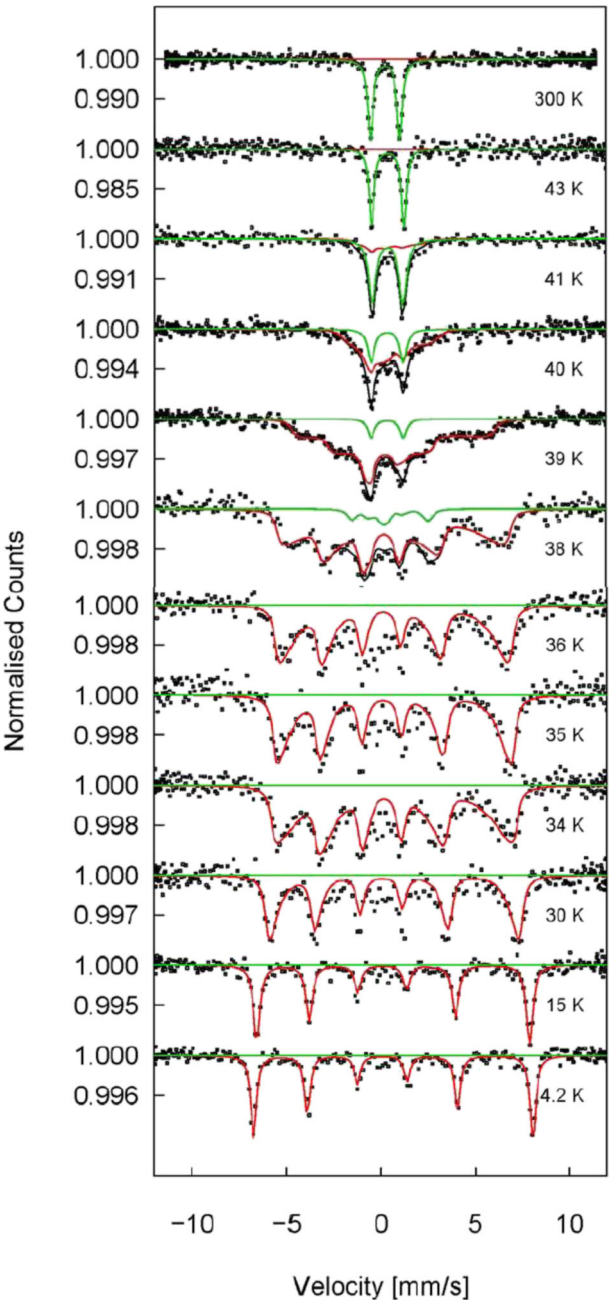

Fig. 2 Representative ^{57}Fe-Mssbauer spectra for o-Yb($Mn_{0.995}Fe_{0.005}$)O_3. The fitted theory curve is the sum of a magnetic sextet (*red*) and a paramagnetic doublet (*green*)

transition at $T_N\prime \approx 36$ K. However, there is also an increasing asymmetric line broadening. Following our approach used for h-$YbMnO_3$ [3], reasonable fits have been achieved using the model devised by Bocquet et al. [12, 13]. In principle, their model is based on

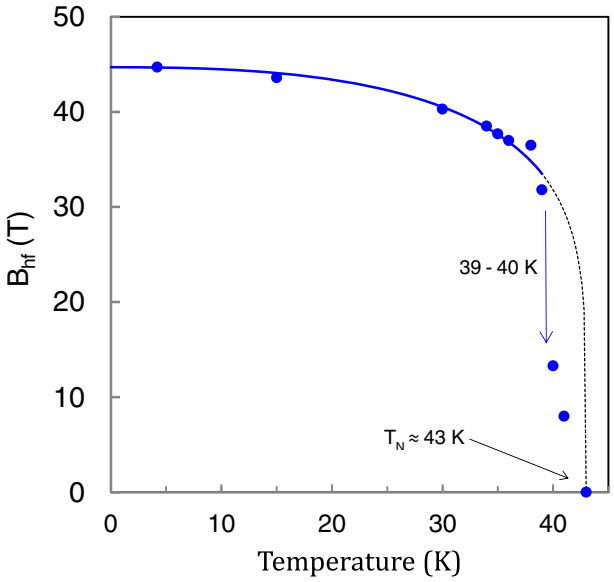

Fig. 3 Temperature dependence of the maximum magnetic hyperfine field, B_{hf}, determined for the ^{57}Fe probe nucleus in o-Yb($Mn_{0.995}Fe_{0.005}$)O_3

slow relaxation of a large magnetic cluster, which is an unlikely scenario in this present work. However, in practice, it is equivalent to a Boltzmann-like distribution of B_{hf} values up to their maximum cut-off value and provides a useful representation of the asymmetric magnetic spectra.

Finally, in the temperature range of the incommensurate magnetic phase (36 K < T < 43 K), there is a superposition of the two phases. The intensity of the paramagnetic doublet decreases with decreasing temperature and it seems to undergo weak magnetic broadening. This phase appears to persist down to an even lower temperature of about 35 K. However, the statistics in the central region of the spectra do not support a detailed analysis at these temperatures. The magnetic sub-spectrum decreases in intensity with increasing temperature and the magnetic splitting collapses over the relatively narrow temperature range of 39 – 40 K. The collapse of the magnetic splitting is more evident in Fig. 3 where the maximum B_{hf} value associated with the asymmetric magnetic broadening is plotted as a function of temperature. Below 39 K, its gradual decrease with increasing temperature is similar to what was observed for the ^{57}Fe-doped hexagonal phase h-$YbMnO_3$ [3]. In that case it was described by an empirical relationship of the form $B_{hf} = B_{hf}(T=0)(1–(T/T_N)^{\alpha})^{\beta}$. For comparison, a similar curve (with $\alpha = 2.52$ and $\beta = 0.19$) has been drawn through the data in Fig. 3 (4.2 to 39 K, solid blue line) and extrapolated to $T_N = 43$ K (broken blue line). At T $\approx$ 39 – 40 K, the maximum B_{hf} value departs from the empirical curve and drops sharply to less than half value, before falling less rapidly to zero at $T_N \approx 43$ K. It is interesting to note that thermal hysteresis, often associated with first-order transitions, was observed for the o-$YbMnO_3$ specific heat data recorded by Tachibana et al. [1]. However, it was centred on the commensurate-incomensurate magnetic transition at $T_{N'} \approx 36$ K.

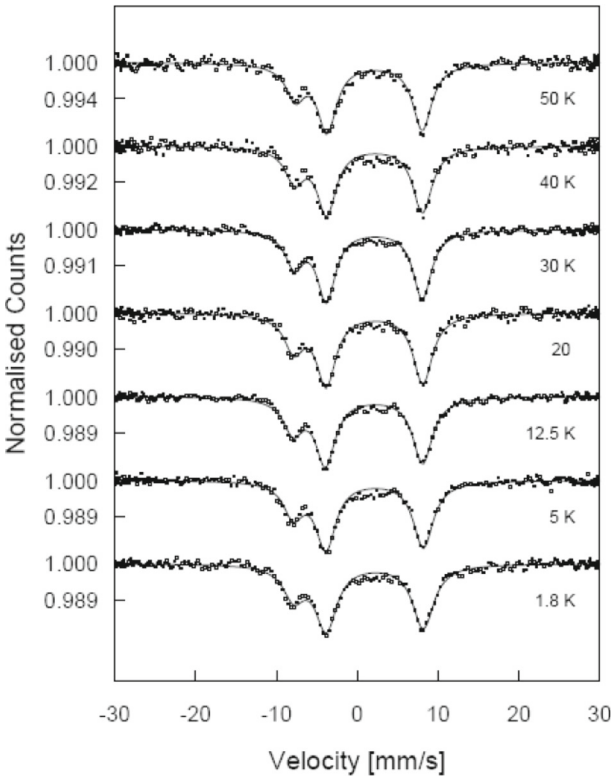

Fig. 4 Representative ^{170}Yb-Mössbauer spectra for undoped o-$YbMnO_3$. The fitted theory is represented by the *solid line*

The ^{170}Yb-Mössbauer spectra are shown in Fig. 4. There is no evidence of magnetic splitting and the spectra were all fitted with a pure axial ($\eta = 0$) quadrupole interaction. However, it is evident from the temperature dependence of the fitted line width, Γ, in Fig. 5 (bottom left inset) that there is a more subtle effect of line broadening which increases with decreasing temperature. Nevertheless, the absence of a well-defined, magnetically-split, five-line spectrum indicates that there is still only a very weak exchange field acting at the Yb site. The quadrupole interaction strength, eQV_{zz}, also increases smoothly from 31.4 mm s^{-1} at 50 K to a maximum of 32.2 mm s^{-1} at 5 K as the temperature decreases (Fig. 5). This is a very small change and suggests that the situation is one of a well-isolated Kramers doublet ground state (leading to negligible thermal population of the excited states). In support of this, the tentative CF parameters derived in Section 3, give a CF scheme with the next excited Kramers doublet at about 148 K above the ground state doublet (top right inset in Fig. 5). A theoretical simulation of the quadrupole interaction strength as a function of temperature indicates that it should increase gently from 20.1 mm s^{-1} at 50 K to 22.3 mm s^{-1} at 1 K. The trend is similar but the absolute values are too small.

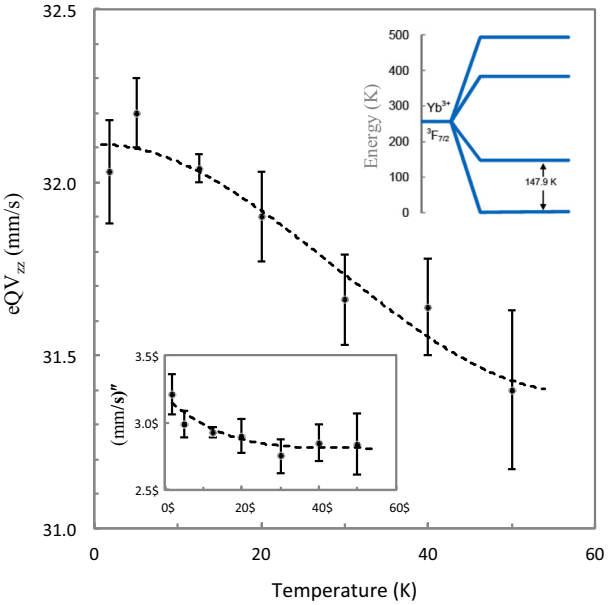

Fig. 5 ^{170}Yb-Mössbauer quadrupole interaction strength, eQV_{zz}, as a function of temperature for o-$YbMnO_3$. Also shown are the line width data (bottom left) and a tentative Yb^{3+}CF scheme (top right)

5 Conclusions

Doped ^{57}Fe-Mössbauer is demonstrated to provide a useful probe of the Mn sub-lattice magnetization in orthorhombic o-$YbMnO_3$. In conjunction with a simple point charge model estimation of the EFG tensor, the ^{57}Fe-Mössbauer results are consistent with a low temperature E-type antiferromagnetic order where the Mn moments are aligned with the *a*-axis (Pnma setting). However a puzzling first order behaviour, with a sharp variation in the magnetic hyperfine field, is observed in the mid temperature range of the incommensurate phase. According to ^{170}Yb-Mössbauer results for pure o-$YbMnO_3$, the Yb sub-lattice does not order magnetically in its own right down to 1.8 K.

Acknowledgments GAS acknowledges the generous hospitality of the McGill University, HAS acknowledges her UIPA and UCPRS scholarships at UNSW Canberra, and DHR acknowledges his UNSW Canberra Rector-Funded Visiting Fellowship. This work was supported in part by grants from the Natural Sciences and Engineering Research Council of Canada and Fonds de Recherche sur la Nature et les Technologies, Quebec. The ^{170}Yb source activations were carried out by M Butler at the McMaster Nuclear Reactor (MNR), Hamilton, Ontario.

References

1. Tachibana, M., Tomotaka, S., Kawaji, H., Atake, T., Takayama-Muromachi, E.: Phys. Rev. B **75** (2007)
2. Huang, Y.H., Fjellvag, H., Karppinen, M., Hauback, B.C., Yamauchi, H., Goodenough, J.B.: Chem. Mater. **18**, 2130–21 (2006) **19**, 2139 (2007)
3. Salama, H.A., Stewart, G.A., Ryan, D.H., Elouneg-Jamroz, M., Edge, A.V.J.: Phys. J. Condens. Matter **20**, 255213 (2008)
4. Shannon, R.D.: Acta. Crystallogr. A **32**, 751–767 (1978)

5. Lauer, S., Marathe, V.R., Trautwein, A.: Phys. Rev. A **19**, 1852–1861 (1979)
6. Su, Z., Coppens, P.: Acta. Cryst. A **52**, 748–756 (1996)
7. Chappert, J., Frankel, R.B., Misetich, A., Blum, N.A.: Phys. Lett. B **26**, 406-407
8. Stevens, J.B.: Table of Nuclear Moments. In: J.W. Robinson (ed.): CRC Handbook of Spectroscopy, 32nd ed., Vol 3, p. 467. CRC Press, Boca Raton, Florida
9. Dufek, P., Blaha, P., Schwarz, K.: Phys. Rev. Lett. **75**, 3545–3548 (1995)
10. Schwerdtfeger, P., Sohnel, T., Pernpointner, M., Laerdahl, J.K., Wagner, F.E.: J. Chem. Phys. **115**, 5913–5924 (2001)
11. Diviš, M., Hölsä, J., Lastusaari, M., Litvinchuk, A.P., Nekvasil, V.: J. Alloys Comp. **451**, 662–665 (2008)
12. Bocquet, S., De Grave, E.: Phys. J. Condens. Matter **6**, 6825–6832 (1994)
13. Bocquet, S., Pollard, R.J., Cashion, J.D.: Phys. Rev. B **46**, 11657–11664 (1992)